JACS
JOURNAL OF THE AMERICAN CHEMICAL SOCIETY

Article

pubs.acs.org/JACS

Atomic Imaging of the Irreversible Sensing Mechanism of NO_2 Adsorption on Copper Phthalocyanine

Jun Hong Park,[†] James E. Royer,[‡] Evgeniy Chagarov,[‡] Tobin Kaufman-Osborn,[†] Mary Edmonds,[†] Tyler Kent,[†] Sangyeob Lee,[‡] William C. Trogler,[‡] and Andrew C. Kummel*[,‡]

[†]Materials Science and Engineering Program and [‡]Departments of Chemistry and Biochemistry, University of California, San Diego, 9500 Gilman Drive,, La Jolla 92093, California, United States

Supporting Information

ABSTRACT: Ambient NO_2 adsorption onto copper(II) phthalocyanine (CuPc) monolayers is observed using ultrahigh vacuum (UHV) scanning tunneling microscopy (STM) to elucidate the molecular sensing mechanism in CuPc chemical vapor sensors. For low doses (1 ppm for 5 min) of NO_2 at ambient temperatures, isolated chemisorption sites on the CuPc metal centers are observed in STM images. These chemisorbates almost completely desorb from the CuPc monolayer after annealing at 100 °C for 30 min. Conversely, for high NO_2 doses (10 ppm for 5 min), the NO_2 induces a fracture of the CuPc domains. This domain fracture can only be reversed by annealing above 150 °C, which is consistent with dissociative chemisorption into NO and atomic O accompanied by surface restructuring. This high stability implies that the domain fracture results from tightly bound adsorbates, such as atomic O. Existence of atomic O on or under the CuPc layer, which results in domain fracture, is revealed by XPS analysis and ozone-dosing experiments. The observed CuPc domain fracturing is consistent with a mechanism for the dosimetric sensing of NO_2 and other reactive gases by CuPc organic thin film transistors (OTFTs).

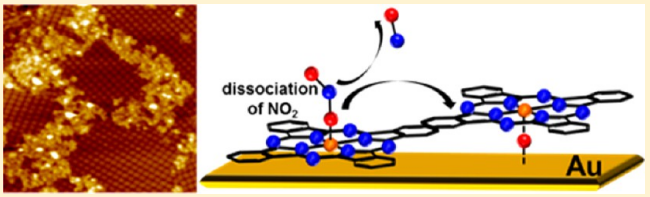

1. INTRODUCTION

Metal phthalocyanines (MPcs) have been used widely for organic thin film transistor (OTFT) gas sensors.[1−6] The MPc films can be deposited readily on inorganic substrates by various techniques including vapor deposition, spin coating, and spray coating. While other organic thin films may have higher mobilities, MPcs are robust under ambient conditions and possess high thermal stability, properties which make them attractive sensor materials. For example, MPcs can maintain their molecular structure at temperatures exceeding 400 °C, and only a few strong acids and oxidizing agents are able to decompose MPcs. The electronic properties of MPcs can be modified by replacing the central metal atom or adding functional groups to the phthalocyanine rings. Structural and electronic properties of single MPc molecules and MPc monolayers on solid surfaces have been investigated by a few research groups.[7−13]

MPc molecules can act as electron donors due to their delocalized π-electrons which are readily ionized, behave as p-type semiconductors, and provide a basis for chemiresistive sensing.[1,14,15] The low ionization energy of MPcs imparts low activation energy for formation of charge transfer complexes with oxidizing gases. The charge distribution in the MPc molecule is also not uniform.[16,17] The nitrogen atoms around the central metal atom have a relatively high electron density, while the inner carbon atoms have an electron density lower than that of the outer aromatic carbon atoms.[8,9] Consequently, charge transfer reactions of MPcs with electron-acceptor gases are strongly favored to occur on the central metal atom rather than at other sites.[1]

Detection of electron-accepting analytes by MPc OTFTs is governed primarily by reaction between the metal center and analytes that, in a simplified model, act as "dopants":[18,19] Pure MPc films are insulating in vacuum, but they become p-type semiconductors when exposed to dopant gases.[1,18−20] The induced p-type conductivity of MPc films has been modeled as formation of charge transfer complexes on the metal centers with oxidative dopants. Weak oxidative analytes (such as O_2)[4,19] chemisorb weakly on MPc films as electron acceptors and form superoxide adducts consisting of oxidized MPc^+ and O^{2-} species; holes are injected into the bulk solid from the positively charged MPc^+. The injection of these holes moves the valence band (HOMO) edge toward the Fermi level, forming a p-type MPc film.[1] Electron paramagnetic resonance (EPR) and electron spin resonance (ESR) studies have shown the presence of these superoxide adducts directly on MPc.[21−23]

Sensors based on MPcs have higher chemical sensitivities and longer recovery times for strong-binding analytes (NO_2, O_3, H_2O_2, and NO) than those for weak binding analytes.[3,24−30] Weak binding analytes induce weak charge transfer reactions and have fast reversible recovery times. For low doses, tight-binding dopants also show reversible recovery, but for high doses, tight-binding analytes (for example NO_2[2,24,31−33] or

Received: April 15, 2013

   dx.doi.org/10.1021/ja403752r | J. Am. Chem. Soc. XXXX, XXX, XXX−XXX

NO[29,30]) have strong charge transfer reactions on MPc films, and the recovery times are very slow or irreversible. In practical sensing devices, weak-binding analytes cannot be ignored because ambient air contains a high concentration of two such analytes, O_2 and H_2O. In order to adsorb on MPc, the strong binder NO_2 must initially compete for reaction sites with gaseous or bound O_2 and H_2O that are present at much higher concentrations. When MPc is dosed with NO_2, it should bind tightly to MPc.[1,2,34] However, when NO_2 dosing ceases, the high background of O_2 and H_2O will compete and cause the NO_2 to desorb if it is reversibly bound. This competition model is consistent with strong-binding analytes having reversible binding to MPc for very low analyte doses. However, the irreversible behavior observed for strong-binding gaseous oxidants on MPc surfaces and their ability to induce charge accumulation in the MPc film are not fully understood on the molecular scale.[35]

The present study uses molecular-scale imaging and chemical spectroscopy to investigate the irreversible sensing response of CuPc OTFTs exposed to NO_2 gas pulses at ambient temperatures in air. Previously, it was shown that H_2O_2 vapor doses of high concentration induce an unrecoverable threshold voltage shift which is consistent with an irreversible sensor response.[28] NO_2 is another strong-binding gaseous oxidant; therefore, it is also expected to show an irreversible sensing threshold voltage shift on the CuPc surface. In order to investigate the sensing response, CuPc OTFT sensing measurements are performed during exposures to a mixture of NO_2 and synthetic air. To understand the NO_2 dosimetric sensing behavior on a molecular level, scanning tunneling microscopy (STM) has been employed to image physical changes in the MPc surface that are induced by NO_2 binding.

2. EXPERIMENTAL DETAILS

Bottom-gate, bottom-contact CuPc OTFTs were prepared by photolithography. The source and drain electrodes were deposited by electron beam evaporation onto $SiO_2/n^{+2}Si(100)$ substrates (Silicon Quest). The 100 nm thermally grown SiO_2 layer acts as a gate oxide with C_{ox} = 34.5 nF cm^{-2}. The channel width ($W = 10^5$ μm) and length (L = 5 μm) are constant for all OTFTs. Deposition of 5 nm Ti was used as an adhesion layer for the 45 nm Au electrodes and electrical contact pads. A four-monolayer CuPc film was deposited on the OTFT substrate under ultrahigh vacuum with the use of molecular beam deposition. The deposition rate was approximately 1 Å s^{-1}. The devices were wire-bonded onto a ceramic, dual in-line package (DIP) and mounted on a printed circuit board for NO_2 sensing. Current−voltage (I−V) measurements were recorded in situ during NO_2 vapor dosing. The I−V data for the OTFTs were analyzed every 60 s by a gate voltage (V_g) sweep from +10 to −10 V at 4 V s^{-1} with the drain voltage (V_{ds}) held at −10 V. A National Instruments PXI-6259 M-series multifunction DAQ controlled by a custom-designed LabVIEW program was used for voltage sweeps and data acquisition. The threshold voltage (V_{th}) and mobility (μ) were calculated from a linear fit to the equation for OTFT drain current in the saturation regime (eq 1).

$$\sqrt{I_d(\text{sat})} = \sqrt{\frac{W\mu C_{ox}}{2L}}(V_g - V_{th}) \quad (1)$$

The V_{th} and μ calculations were performed in real time during sensing and used a constant range of fit for the gate voltage (V_g) of $-10\ \text{V} \le V_g \le -7\ \text{V}$. All OTFT sensing experiments were performed with zero grade air (Praxair, <2 ppm H_2O, <0.02 ppm NO_2) and a 10 ppm NO_2 mixture in dry air (Airgas).

Deposition of copper phthalocyanine (CuPc) was performed in a multichamber Omicron ultrahigh vacuum (UHV) system with a base pressure below 1 × 10^{-10} Torr. The surface of single-crystal Au(111) at 25 °C was cleaned by sputtering with a 1 keV Ar^+ ion beam (RBD Instruments) with an Ar background pressure of 6 × 10^{-5} Torr. After sputtering, the Au(111) sample was annealed at 500 °C for 30 min for curing. Sputtering and annealing were repeated until STM imaging verified an atomically flat Au(111) surface.

The CuPc was purchased from Sigma Aldrich and purified by multiple sublimations. The sample was prepared by depositing thick overlayers of CuPc on a clean Au(111) surface at 100 °C by organic molecular beam epitaxy with use of a differentially pumped effusion cell (Eberl MBE-Komponenten), while the sample was in the UHV preparation chamber. Subsequently, this multilayer was heated to 350 °C for 4 min, and a flat-lying monolayer of CuPc was formed on the Au(111) surface because the CuPc/CuPc interaction in multilayers is weaker than the CuPc/Au surface interaction.[36] The monolayer structure was confirmed by STM, which showed the characteristic Au(111) herringbone reconstruction through the single-monolayer CuPc films. The monolayer samples were transferred from the preparation chamber via the load lock and introduced into the atmosphere for NO_2 dosing.

High-concentration NO_2 dosing was performed with a 10 ppm NO_2 in dry synthetic air mixture onto CuPc monolayers at atmospheric pressure. These high-concentration dosing studies were performed in an airtight container with a constant flow of the 10 ppm NO_2 mixture. Low-concentration dosing (1 ppm NO_2 in dry synthetic air) was performed in an airtight, custom-designed flow system with constant flow using mass-flow controllers. The 10 ppm NO_2/air mixture was diluted 10-fold in synthetic air (Praxair, <2 ppm H_2O, <0.02 ppm NO_2) using a separate dilution line to create a 1 ppm NO_2 mixture in synthetic air.

Dosed samples were returned to the UHV chamber through a load lock. The pump down time was limited to 15 min in order to minimize desorption of analytes. Once in UHV, the samples were transferred immediately to the manipulator, which was maintained at −120 °C to minimize analyte desorption. Finally, the −120 °C samples were transferred to the analysis chamber sample stage at −180 °C; the analysis chamber contained an Omicron VT AFM/STM with a base pressure below 5 × 10^{-11} Torr. All STM images were acquired using electrochemically etched W tips.

A monochromatic XPS (XM 1000 MkII/SPHERA, Omicron Nanotechnology) was employed to examine the surface elements and the ratio of their relative intensities. The XPS was operated in a constant analyzer energy mode with the pass energy of 50 eV and the line width of 0.1 eV, using an Al Kα source (1486.7 eV). The takeoff angle was 30° from the sample surface with an acceptance angle of ±7°. The peak analysis process was performed using *CASAXPS* v2.3. The relative XPS intensity of each core-level spectra (C 1s, N 1s, O 1s, and Cu $2p_{3/2}$) was quantified by calculating the peak area divided by the XPS sensitivity factor.

In order to identify adsorbates on the CuPc layer, flash desorption mass spectrometry was performed by mass spectrometry (Max-LT300 with Axial Ionizer, Extrel) in the UHV chamber. The sample temperature was raised from 25 to 300 °C by a pyrolytic boron nitride heater (PBN heater), and the heating speed was 1−2 °C min^{-1}. All signals from 5 m/z to 130 m/z were collected by the Merlin Automation Data system. Note that this flash desorption mass spectrometry is not temperature-programmed desorption, because the heating speed was neither fast nor constant.

Both O_3 and NO were dosed on the CuPc monolayer in the UHV chamber at room temperature with the use of a pulsed supersonic molecular beam source (General Valve series 1), which was triple differentially pumped using a three-chamber source with turbo-molecular pumps. The O_3 was produced from pure O_2 with the use of an ozone generator (AZCO Industries Ltd.). The O_3 generation and persistence after transport through the supersonic beam source was confirmed by mass spectrometry (Max-LT300 with Axial Ionizer, Extrel). The NO analyte was diluted by He (He: 95%; NO: 5%). The pulsed molecular beam operated at 30 Hz with a 100 μs opening time. During dosing, the preparation chamber was pumped only with a turbomolecular pump (TMP). Although beam frequency and dosing

dx.doi.org/10.1021/ja403752r | J. Am. Chem. Soc. XXXX, XXX, XXX−XXX

duration were identical in both NO and ozone dosing, there was a pressure difference in the preparation chamber. The pressure was 2×10^{-9} Torr during ozone dosing, but was 2×10^{-7} Torr during NO dosing. This difference results from the He in the NO mixture which causes back streaming in the TMP.

All DFT simulations were performed with the *Vienna Ab-Initio Simulation Package* (VASP)[37,38] using projector augmented-wave (PAW) pseudopotentials (PP)[39,40] and the PBE (Perdew–Burke–Ernzerhof) exchange-correlation functional.[41,42] The choice of PBE functional and PAW PP was validated by parametrization runs demonstrating good agreement with experimental properties of bulk Au and C, as well as N_2 and O_2 molecular properties. The atomic charges for calculated systems were obtained by applying Bader charge decomposition.[43−45] Note that Bader charge is a value reflecting the number of excess valence electrons (total electrons less absolute value of the nuclear charge) associated with particular atoms; therefore, atoms with positive Bader charge have an absolute negative charge.

3. RESULTS

3.1. Dual Sensing Response of CuPc OTFT to NO_2 Gas Pulses of Variable Duration. The sensing experiments are presented prior to the STM experiments to show the macroscopic evidence of irreversible NO_2 chemisorption via dosimetric sensing. Figure 1 shows typical conductive OTFT sensing responses of CuPc to 100 ppb NO_2 gas pulses of variable duration (30 s, 2 min, 5 min, and 10 min) at 25 °C. During these experiments, high-purity dry air was used as both the purge and the carrier gas. Full $I-V$ curves are measured at each point in time so that the influence of the analyte on the mobility and threshold voltage can be measured independently. The NO_2 doses in these sensor measurements are smaller than in the STM studies, since the $I-V$ characteristics are closer to ideal for small doses, thereby enabling independent measurement of the mobility and threshold voltage. Furthermore, a fixed charge of less than 0.1% of a monolayer ($10^{12}/cm^2$) is readily detected by $I-V$ measurement, which is well below the limit of STM detection for almost any adsorbate. The CuPc OTFT has a nonlinear sensing response with increasing dosing time. Analyte-induced changes in the carrier trap energy or carrier density are typically reflected by changes in the mobility, while analyte-induced changes in fixed charge are reflected by changes in the threshold voltage.

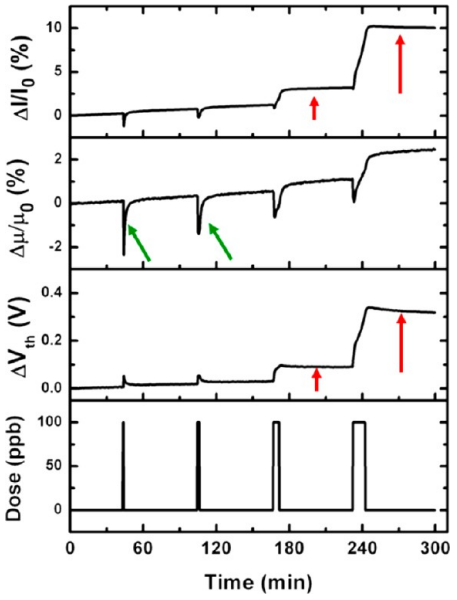

Figure 1. Conductive sensing response of CuPc OTFTs to 100 ppb of NO_2 gas pulses of variable duration. The pulses were 30 s, 2 min, 5 min, and 10 min, resulting in integrated doses of 0.05−1 ppm min^{-1}. Full $I-V$ characterization was performed at each time point to extract the threshold voltage and mobility. For low doses there is a reversible change in mobility (green arrow), while for high doses there is an irreversible shift in threshold voltage (red arrow).

For short analyte pulses (30 s and 2 min), large mobility decreases and possibly small V_{th} shifts are observed, but both the mobility decreases and small V_{th} shifts are reversed when NO_2 dosing ceases during the dry air flow. However, for longer doses (5 and 10 min), large V_{th} shifts occur, and these shifts are irreversible and dosimetric (red arrow). This is consistent with an analyte-induced change in fixed charge. Consequently, both reversible and irreversible components of the sensing mechanism are present. Note that the current (I_d(sat)), which has negative values for p-type transistors, increases with increasing dose of NO_2 because the current is proportional to the square of the threshold voltage (V_{th} increases → current increases), as shown in eq 1. It is also noted that, as more NO_2 is dosed on the CuPc layer, a larger hole carrier density can be generated. The larger positive charge carrier density leads to a source-drain current increase. This increase of charge carrier density can result in domain boundaries, which traps charge carriers being filled.[46] Therefore, the positive charge carriers can move through domain boundaries without being trapped. As a result, an increase of charge carriers can result in an increase in the mobility.

The DFT VASP plane wave calculations show that the adsorption energies of NO and NO_2 on CuPc are very low: (NO_2/CuPc: 0.06 eV and NO/CuPc: 0.02 eV). This was checked by calculating the adsorption energy of NO on a more reactive MPc. For NO/CoPc, the DFT VASP plane wave calculation gives a binding energy of 1.57 eV, which agrees well with the binding energy of 1.55 eV calculated by Nguyen et al.[47] for the same system, which also used the VASP plane wave code. It is noted that other computational methods give slightly higher binding energies; atomic-orbital *DMol* simulations of Lozzi et al. showed a binding energy of 0.40 eV for NO_2/CuPc.[48] The very low adsorption energies of NO and NO_2 on CuPc are consistent with another chemisorbate being the main factor for irreversible changes in the fixed charge in the film. Conversely, the DFT models of weakly bound molecular chemisorption of NO_2 and NO on CuPc are consistent with the observed low-dose reversible changes in mobility. The high doses result in irreversible changes in the film electronic properties, which are consistent with a strong binding reaction. Thus, nondissociative NO_2 adsorption, which has a weak interaction with the Cu metal center, cannot explain the irreversible V_{th} shifts. The data are instead consistent with a secondary effect from NO_2 dosing being responsible for the irreversible component of sensing.

3.2. Morphology Changes in CuPc Monolayers Induced by Dosing NO_2. A CuPc monolayer dosed with NO_2 was imaged in UHV-STM in order to observe the change induced as a result of NO_2 dosing. Exposure of the CuPc monolayer to small doses of NO_2 results in weakly bound chemisorbates on the metal centers of the CuPc molecules. In Figure 2a, bare CuPc molecules form a highly ordered monolayer on Au (111) with four-fold symmetry. The inset image shows individual CuPc molecules on the Au(111). A schematic molecular structure of CuPc is also presented in Figure 2b. The molecular structure is clearly defined in the inset

dx.doi.org/10.1021/ja403752r | J. Am. Chem. Soc. XXXX, XXX, XXX−XXX

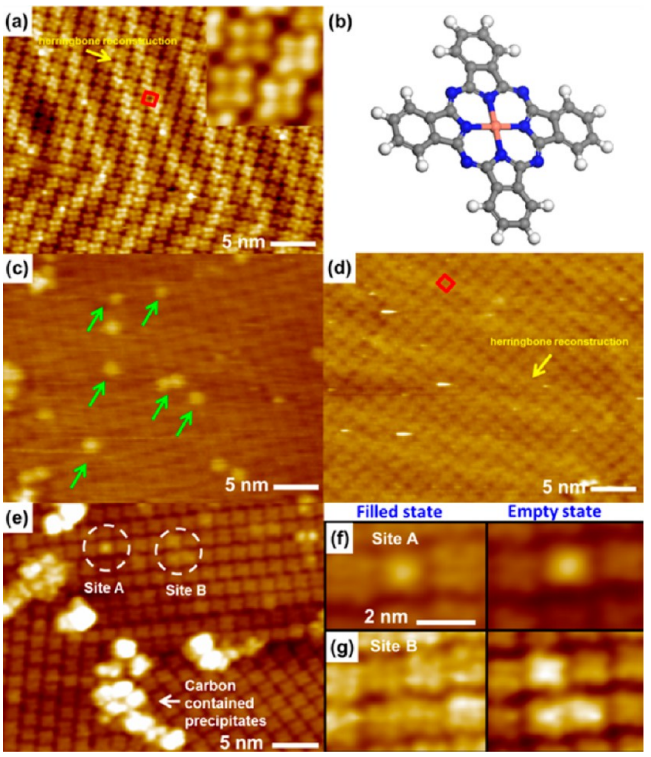

Figure 2. Empty-state STM images (a–e: V_s = 2.0 V, I_t = 40 pA) of a CuPc monolayer. (a) Clean CuPc surface. Inset image shows individual CuPc molecules. (b) Schematic molecular structure of CuPc (pink ball Cu; blue ball N; gray ball C; white ball H). (c) After dosing 1 ppm NO_2 for 5 min at 25 °C, then annealed at 50 °C for 20 min. Green arrows indicate chemisorbates. (d) After dosing 1 ppm NO_2, then annealing at 100 °C for 30 min. (e) After dosing 10 ppm NO_2 for 5 min at 25 °C, then annealing at 50 °C for 20 min. (f) Filled- and empty-state STM images of site A in (e). (g) Filled- and empty-state STM images of site B in (e). (f and g: V_s = ± 1.0 V, I_t = 40 pA.) Note dosing NO_2 of 1 ppm for 5 min is referred to as low dose (c and d), while dosing NO_2 of 10 ppm for 5 min is referred to as high dose (e, f, and g).

STM image; the holes or dark sites correspond to the Cu atom in the center of each CuPc molecule, and aromatic rings are visible as a bright four-leaf pattern.[8] After dosing NO_2 (1 ppm for 5 min: low dose) and annealing at 50 °C to improve STM imaging, the images reveal small NO_2-induced chemisorption sites dispersed on the CuPc layer (Figure 2c). Note that "NO_2 chemisorption site" denotes the site formed by NO_2 dosing, as shown in Figure S1 in the Supporting Information (SI). All DFT models show that single gaseous molecules preferentially bind to the metal centers of CuPcs, which is consistent with the NO_2 low-dose STM images.[47,49,50] STM experiments show that these chemisorbates desorb from the CuPc monolayer after annealing at 100 °C for 30 min in Figure 2d. It is noted that, although there is a resolution difference between a and d of Figure 2, CuPc molecules form a crystal structure which has four-fold symmetry in both a and d of Figure 2 (red rectangle). In addition, the Au(111) herringbone reconstruction (yellow arrow) is observed through the single-monolayer CuPc films as a strip in both a and d of Figure 2. It is also noted that the orientation of herringbone reconstruction can be altered by the Au atomic steps. These chemisorbates also are observed for high coverage of NO_2 dosed onto the CuPc monolayer (10 ppm for 5 min). In Figure 2e, two different chemisorption sites are shown, and each site has a distinct bias dependence (Figure 2f and g). It is noted that precipitates are observed on the domain boundaries of the CuPc monolayer, which were shown to be mostly carbon via XPS, as shown in Figure S2 in the SI. The precipitates could also be mixtures of carbon complex and displaced CuPc molecules. It is hypothesized that these precipitates originate from exposure to lab air. For site A, the metal center is brighter than the aromatic ring in both the empty- and filled-state images. However, for site B, the entire CuPc molecule is darker than the ambient CuPc in the filled-state image and is brighter in the empty-state image. However, as explained below, for high NO_2 exposure there are subsurface chemisorbate species which may influence the electronic structure of the CuPc layer, and thereby create the diversity of observed isolated chemisorption sites. It is noted that the chemisorbates in Figure 2c are mostly isolated and dispersed on CuPc monolayer. On the other hand, approximately only 27% of the chemisorption sites B in Figure 2e exist as isolated sites. Furthermore, chemisorbates in Figure 2c do not have bias dependence, while chemisorbates B in Figure 2e show distinct bias dependence, as shown in Figure 2g.

Monolayer CuPcs can maintain their crystal structure in ambient air. Before dosing NO_2 gas, CuPc molecules form large, highly ordered domains on each Au(111) step as shown in Figure 3a. Figure 3a shows CuPc molecules form monolayers

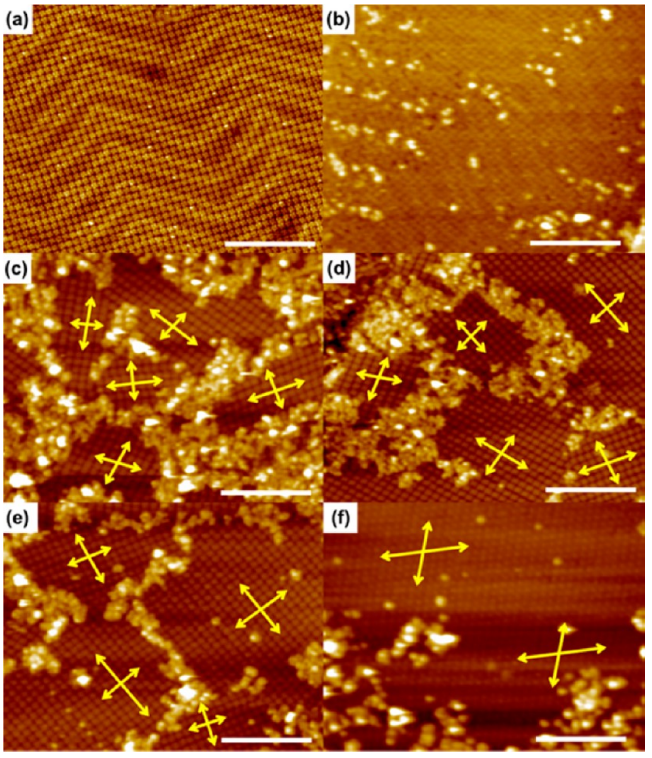

Figure 3. Empty-state STM images of a CuPc monolayer surface. Scale bars are 20 nm. (a) Clean CuPc monolayer surface (V_s = 2.0 V, I_t = 10 pA). (b) CuPc mononolayer exposed to air for 30 min and annealed at 50 °C for 10 min (V_s = 2.0 V, I_t = 20 pA). (c) after dosing 10 ppm NO_2 for 5 min and annealed at 50 °C for 10 min (V_s = 2.0 V, I_t = 40 pA). (d) CuPc monolayer from (c) annealed at 50 °C for an additional 10 min (V_s = 2.0 V, I_t = 40 pA). (e) CuPc monolayer from (d) annealed at 50 °C for an additional 50 min (V_s = 2.0 V, I_t = 40 pA). Image (e) is slightly distorted due to thermal drift. Yellow arrows indicate the orientation of CuPc domains. Note dosing of 10 ppm NO_2 for 10 min is referred to as high dose. (f) CuPc monolayer from (e) annealed at 150 °C for further 6 h (V_s = 2.0 V, I_t = 40 pA).

dx.doi.org/10.1021/ja403752r | J. Am. Chem. Soc. XXXX, XXX, XXX–XXX

having large domain sizes. When the CuPc monolayer is exposed to air for 30 min, reorganization of molecules and fractured domains are not observed, even though some carbon-rich adsorbates from ambient air are observed on the monolayer CuPc surface (Figure 3b).

In order to determine the mechanism of the irreversible dosimetric sensing response, higher concentrations of NO_2 were dosed on the CuPc monolayer surface. After dosing with 10 ppm of NO_2 for 5 min on the CuPc monolayer surface, reorientation of CuPc molecules and fractured domains are observed. As shown in Figure 3c and d, after 10 ppm of NO_2 is dosed at 25 °C for 5 min (high dose) and annealed in UHV at 50 °C, new domain boundaries are generated, and the domain sizes become smaller. Predose domains are larger than 200 nm in length and limited by terrace size, while postdose domains are 50−80 nm in length, as shown in Table 1. Therefore, while high dose NO_2 readily induces domain fracture, ambient gaseous molecules do not induce domain fracture.

Table 1. Quantitative Analysis of Domain Size of Mono-, Bi-, and Multilayer CuPcs Dosed with 10 ppm of NO_2 for 5 min, As a Function of Annealing Conditions

	sample	average domain size[a] (nm)	standard error
monolayer	clean surface	332	16
	dosed and annealed at 50 °C, for 10 min	46.8	6
	dosed and annealed at 50 °C, for 20 min	75.6	11
	dosed and annealed at 50 °C, for 1 h 10 min	54.7	4
bilayer	clean surface	357	17
	dosed and annealed at 50 °C, for 1 h	38	4
multilayer	clean surface	279	29
	dosed and annealed at 50 °C, for 1 h	51	4

[a]The average grain size was calculated using the linear intercept method. Once the mean linear intercept was calculated, the result represents the grain-boundary area per unit volume, which was then multiplied by 1.5 in order to approximate the average spherical grain size.

The NO_2-induced domain fracture is not reversible at 25 °C. As shown in Figure 3e, after additional annealing of sample from Figure 3d at 50 °C for over 1 h, the extent of fracture is unchanged, consistent with the domain fracture involving a tightly bound adsorbate. This domain fracture can be recovered by annealing above 150 °C (Figure 3f). In Figure 3f, additional annealing of the sample from Figure 3e at 150 °C induces a larger area of domain, which results from merging with the fractured domain. As shown by the yellow arrows in Figure 3c, d, and e, each fracture domain has a different symmetry direction, which is consistent with nearly all the CuPc having realigned instead of simple decomposition along domain boundaries. This domain fracture in the CuPc monolayers is nearly irreversible at room temperature, which is consistent with the V_{th} shifts observed in the OTFT sensor data at high dosing.

3.3. Domain Fracture-Induced Atomic O on Bilayers and Multilayers of CuPc. A similar domain fracture is observed on bilayer and multilayer CuPc films, after exposure to high NO_2 doses. On clean bilayer surfaces, CuPc molecules form a highly ordered second layer which has an average domain size of 357 ± 17 nm, as shown in Figure 4a and Table 1. After NO_2 is dosed, new domain boundaries are induced on the first and second layer (Figure 4b). However, the second-layer domains are more disordered than the monolayer domains after equivalent NO_2 doses. Note that "disordered" indicates that some defect sites are observed as vacancies. On CuPc monolayers dosed by NO_2, although NO_2 dosing induces domain fracture, CuPc molecules still form a close-packed crystal structure in Figure 3d. However, on a bilayer dosed by NO_2, larger amounts of vacancies are observed. On the NO_2-dosed CuPc bilayers, fractured domains in the first layer are also clearly shown through vacancies in the second layer (Figure 4b and c). The enlarged STM image, Figure 4c, shows that the direction of CuPc molecules arranged in the first layer exactly corresponds with the symmetry of the second layer (symmetry of first layer - green arrow; symmetry of second layer - blue arrow), consistent with the domains having vertical order since the domain fracture is induced at the CuPc/Au(111) interface. It is hypothesized that dissociative chemisorption product atoms, which result from the interaction of NO_2 on the CuPc/Au surface, penetrate the CuPc bilayer and chemisorb on the Au(111). These byproduct atoms at the CuPc/Au(111) interface reorient the first CuPc layer (the CuPc/Au(111) interface), which also results in reorientation of the second CuPc layer while keeping the relative positions of CuPc in layers one and two.

Subsurface reactions also induce reconstruction of domain structure on multilayers. Before NO_2 is dosed, CuPc molecules form smooth and large domain structures on clean multilayer surfaces (Figure 4d), and the herringbone structure of Au(111) can be observed clearly. However, when NO_2 is dosed at 10 ppm for 5 min, small domains appear (Figure 4e). Although the NO_2-dosed multilayer CuPc domains have a high defect density, the CuPc molecules form polycrystalline domain structures similar to the ones observed on the NO_2-dosed CuPc bilayer surface. The average domain size on the NO_2-dosed CuPc multilayer film is 51 ± 4 nm as shown in Table 1. Each domain has a different symmetry of molecular arrangement as shown by the yellow arrow in Figure 4e.

3.4. Chemical Mechanism for Irreversible Behavior. The formation of fractured domains after high NO_2 dosing is consistent with formation of a tightly bound adsorbate which changes the unit cell size of the MPc monolayer.[51] It is hypothesized that this arises from dissociative chemisorption of NO_2 into weakly bound NO and tightly bound atomic O. To identify weakly bound adsorbates, flash desorption mass spectrometry was performed. Figure 5a shows mass spectra of molecules which desorb from a CuPc monolayer dosed with 10 ppm of NO_2 for 5 min as the surface is heated rapidly. The times in Figure 5 indicate the duration of heating prior to recording the spectra at the temperatures denoted. Note that the 18, 28, and 44 m/z peaks correspond with background H_2O^+, CO^+, and CO_2^+, whose parent molecules are always present in the UHV chamber. A 30 m/z peak starts to be detected above 70 °C, and its intensity increases as the surface temperature increases. In nearly all published mass spectra, NO_2 and NO both exhibit 30 m/z peaks, but only NO_2 has a 46 m/z mass component.[52,53] However, in Figure 5b, there is no detectable peak at 46 m/z. Other research groups also report that NO was detected on NO_2-dosed MPc films by IR spectroscopy.[54] The observation of NO by flash desorption mass spectrometry is consistent with NO_2 dissociating to NO and atomic O on the CuPc monolayer and is similar to multiple

dx.doi.org/10.1021/ja403752r | J. Am. Chem. Soc. XXXX, XXX, XXX−XXX

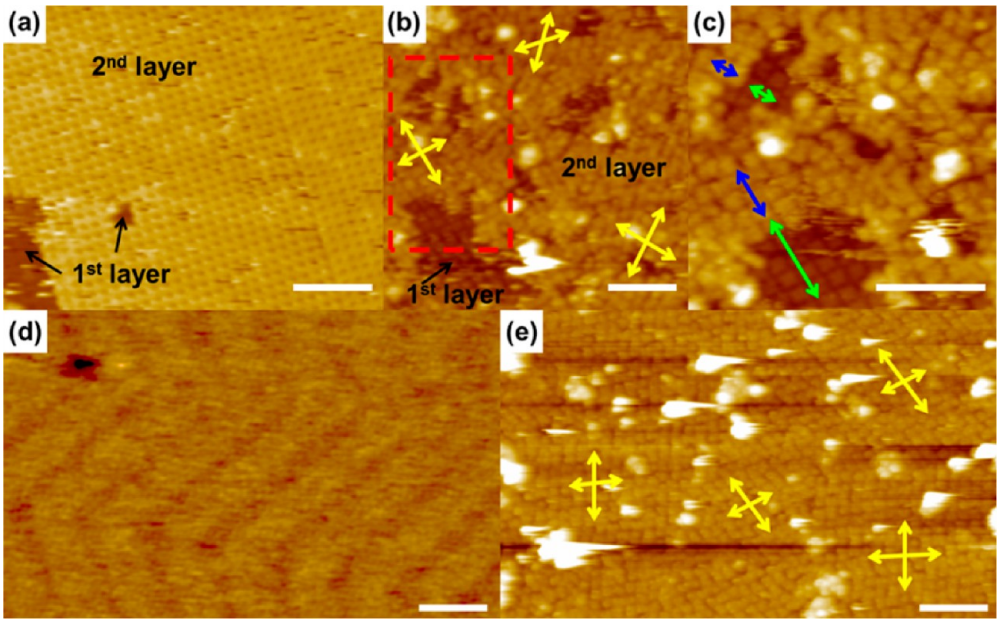

Figure 4. Empty-state STM images of bi- and multilayer CuPc surfaces. Scale bars are 10 nm. (a) Clean CuPc bilayer (V_s = 2.0 V, I_t = 10 pA). (b) CuPc bilayer dosed with 10 ppm NO_2 for 5 min and annealed at 50 °C for 1 h (V_s = 2.0 V, I_t = 20 pA). (c) Expanded STM image from red rectangle in (b). The first layer is shown through the vacancies of the second layer (V_s = 2.0 V, I_t = 20 pA). (d) Clean CuPc multilayer (V_s = 2.0 V, I_t = 10 pA). (e) CuPc multilayer dosed with 10 ppm NO_2 for 5 min and annealed at 50 °C for 1 h (V_s = 2.0 V, I_t = 40 pA). Yellow arrows indicate the orientation of CuPc grains.

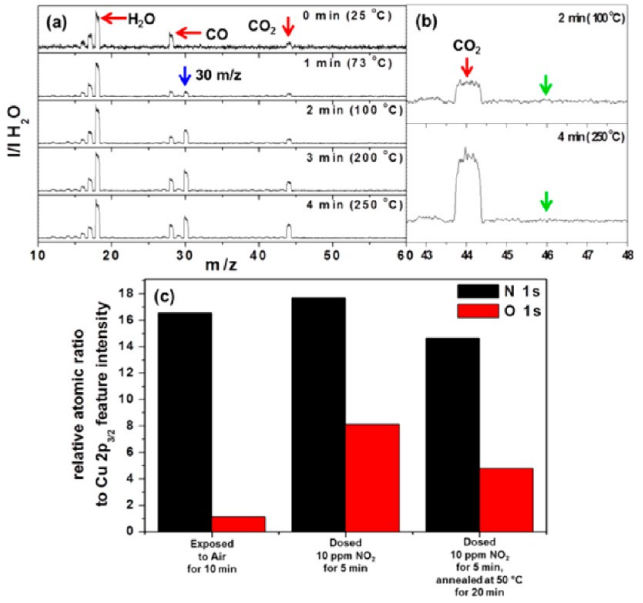

Figure 5. Flash desorption mass spectrometry and XPS analysis of the NO_2/CuPc/Au(111) surface. (a) Flash desorption mass spectrum of gaseous molecules from a CuPc layer dosed with 10 ppm of NO_2 at 25 °C for 5 min. The times indicate the duration of heating prior to recording the spectra at the temperatures denoted in the figure. (b) Expanded spectrum from (a) between 42.5 and 48 *m*/*z*. (c) Coverage of N and O estimated from the relative XPS intensities. Surface concentrations are calculated from the XPS ratios relative to the $Cu2p_{3/2}$ intensity.

reports of NO_2 dissociation to NO + O on various surfaces.[55−57]

A high concentration of O species on CuPc/Au dosed by NO_2 is established by XPS analysis. To obtain the total concentration of O and N species, the XPS peaks for O and N were integrated and normalized to the Cu signal (see below). Figure 5c shows a large increase of the relative ratio of O to Cu on the CuPc monolayer/Au surface after NO_2 is dosed at 10 ppm for 5 min compared with an air-exposed CuPc/Au monolayer surface. On CuPc/Au surfaces dosed with 10 ppm of NO_2 for 5 min and annealed, the relative coverage of O is still 4 times larger than on an air-exposed CuPc/Au monolayer, and the coverage of O decreases with annealing.

Conversely, the integrated nitrogen XPS peak is nearly independent of NO_2 dose; however, since each CuPc contains eight nitrogen atoms, detection of adsorbed nitrogen requires XPS peak shape analysis. In order to identify the chemical binding status of N species, chemical fitting analysis was performed with XPS data which are measured from the CuPc monolayer/Au surface. The XPS N 1s spectra of the CuPc monolayer measured before and after dosing with 10 ppm of NO_2 for 5 min are presented in a and b, respectively, of Figure 6. In Figure 6a, three components are detected on CuPc/Au exposed to only air; 398.1 eV is assigned to the N−Cu bond and 398.6 eV is assigned to the N−C bond.[48] Note the very wide and small peak (400.0 eV) is generated by shake up transitions. It is also noted there is difference in the binding energies between the above data and the reference data, because the above binding energies are measured from a monolayer of CuPc on Au, while the reference data are measured from thick layers of CuPc on Si_3N_4 substrates. After dosing with NO_2, a new component is observed at 398.9 eV, and this component is consistent with the presence of NO_2. It is noted that this NO_2 may be bound to precipitates or displaced CuPc molecules instead of the CuPc monolayer.

By XPS chemical fitting analysis, the presence of O atoms was clarified as shown in c and d of Figure 6. Parts c and d of Figure 6 show the XPS O 1s spectra for the CuPc monolayer measured before and after dosing with 10 ppm of NO_2 for 5 min. CuPc/Au exposed only to air for 10 min shows a weak,

dx.doi.org/10.1021/ja403752r | J. Am. Chem. Soc. XXXX, XXX, XXX−XXX

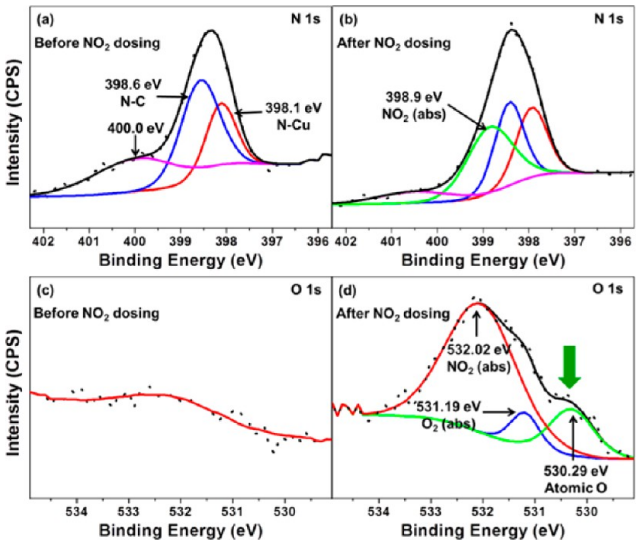

Figure 6. XPS chemical fitting analysis of NO_2/CuPc/Au(111). (a) N 1s spectra taken from CuPc/Au(111) exposed to air for 10 min, (b) N 1s spectra taken from the NO_2/CuPc/Au(111) is dosed with 10 ppm of NO_2 for 5 min and subsequently annealed at 50 °C for 20 min. (c) O 1s spectra taken from CuPc/Au(111) exposed to air for 10 min, (d) O 1s spectra taken from the NO_2/CuPc/Au(111) dosed with 10 ppm of NO_2 for 5 min and subsequently annealed at 50 °C for 20 min.

broad peak from 531.5 to 533.5 eV. This broad peak can result from different oxygen states, for example, O_2 and H_2O. However, after the NO_2 dosing, the main peak is at 532 eV, and a new feature is observed as a shoulder (green arrow). The presence of this shoulder indicates that the dosing with NO_2 induces formation of new O binding states in CuPc/Au. Using peak-fitting procedures, three components were identified (532.0, 531.2, and 530.3 eV) in the O 1s spectra. The largest component (532.0 eV) can be assigned to the oxygen atoms which form as NO_2 anneals on CuPc/Au,[58] and this is also shown in N 1s spectra. Although NO_2 dosing results in low binding energy states of O in CuPc/Au associated with dissociation products, the majority of O still remains with a binding energy consistent with adsorbed molecular NO_2. The second peak (531.2 eV) is consistent with the presence of the O_2, which can be introduced from air during NO_2 dosing or produced during dissociative chemisorption of NO_2.[59] Lastly, the third peak is detected at 530.3 eV; this peak dominates the shoulder of O 1s spectra. The binding energy (530.3 eV) is consistent with atomic O on Au;[60] there is a small difference in the binding energy between 530.3 eV and published data (530 and 530.1 eV) consistent with the atomic oxygen having interactions with both the Au surface and overlying CuPc molecules. As a result of XPS analysis, it is hypothesized that some of NO_2 dosed on CuPc/Au dissociates to atomic oxygen. It is noted that the difference in calculated binding energy between O/Au and CuPc/O/Au is only 0.15 eV. Furthermore, the calculated difference in Bader charge is only 0.09 between O/Au and CuPc/O/Au (O/Au: 6.69 |e|, CuPc/O/Au 6.78 |e|). This small difference in Bader charge may be too small to induce a difference in binding energy in XPS spectra.

Domain fracture induced by atomic O was also confirmed by O_3 dosing experiments, since O_3 dissociatively chemisorbs into O_2 and atomic O.[61] STM images were recorded after O_3 dosing on a CuPc monolayer for 10 min at 25 °C with a supersonic molecular beam source (MBS) (Figure 7a). As a control, NO

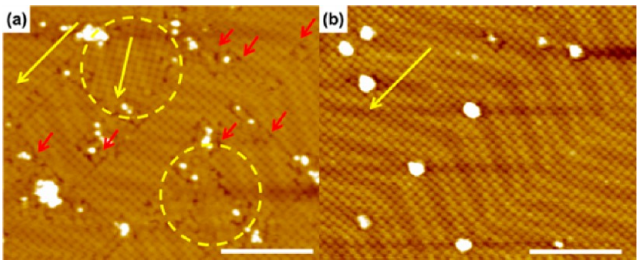

Figure 7. Empty-state STM images of a CuPc monolayer dosed with a supersonic MBS (molecular beam source). Scale bars are 20 nm. (a) CuPc monolayer dosed with ozone (O_3) for 10 min at 25 °C (V_s = 2.0 V, I_t = 20 pA, fMBS = 30 Hz). Red arrows indicate subsurface crack sites. (b) CuPc monolayer dosed with NO for 10 min at 25 °C (V_s = 2.0 V, I_t = 20 pA, fMBS = 30 Hz). Yellow arrows indicate the orientation of CuPc domains.

diluted in He was dosed on a CuPc monolayer by supersonic MBS for 10 min at 25 °C (Figure 7b), since it does not dissociatively chemisorb. In contrast to the results from ambient dosing with NO_2, dosing O_3 and NO with MBS results in a very low density of carbon-rich adsorbates so that more detail is observed. As shown in Figure 7a, dosing of O_3 on a CuPc monolayer generates new domains which are only 15–20 nm, which is consistent with subsurface O sites similar to the ones generated by NO_2 dissociative chemisorption. In addition, O_3 on CuPc induces the formation of crack sites as indicated by the red arrows that may imply a new subsurface chemisorption site. Conversely, the CuPc monolayer dosed with NO shows neither domain fracture nor crack sites.

DFT calculations were performed to determine the energetics of O transfer from CuPc to Au(111), as shown in Figure 8a–c. The reference state was gaseous atomic O. Note that the plane wave VASP technique was employed to determine the bonding of NO_2 to CuPc; it was found that NO_2 bonding through O is slightly more favorable than through N by 0.02 eV, but the binding is so weak that accurate calculations on the transition state would require the use of a hybrid function which is challenging for modeling large systems. However, it is known that NO is able to dissociate on Cu(111) and (100),[62,63] and NO_2 can dissociate on both Cu surfaces and CuPc layers,[1,48,57,64] consistent with NO_2 bond activation having only a modest activation energy barrier. When O atoms bond with the Au surface, there is a high binding energy (E_{bind} = 4.60 eV); this binding energy was calculated by subtracting atomic O and relaxed Au slab total energies from the energy of the relaxed O/Au system. When O bonds to the CuPc on Au(111), the binding energy is modest (E_{bind} = 1.66 eV). When the O atom is bonded between the CuPc and Au(111), the binding energy is calculated to be highest (E_{bind} = 4.76 eV) which is slightly greater than the binding energy of O on clean Au(111). It is noted that the reference states employed in Figure 8 use atomic O in the gas phase O(g), Au(111)(s), and CuPc/Au(111)(s) to calculate the binding energies. The binding energy of O in the O/CuPc/Au and CuPc/O/Au systems was calculated by subtracting the total energies of atomic O and the relaxed CuPc/Au system from the total energy of the relaxed O/CuPc/Au or CuPc/O/Au systems, respectively. The total energies are −819.754 eV, (adsorbed O, i.e O/CuPc/Au) and −822.855 eV. (subsurface O, CuPc/O/Au); therefore, the 3.1 eV difference represents the increased binding of oxygen migrating from the surface site on CuPc to the site between CuPc and Au. Therefore, any O

dx.doi.org/10.1021/ja403752r | J. Am. Chem. Soc. XXXX, XXX, XXX–XXX

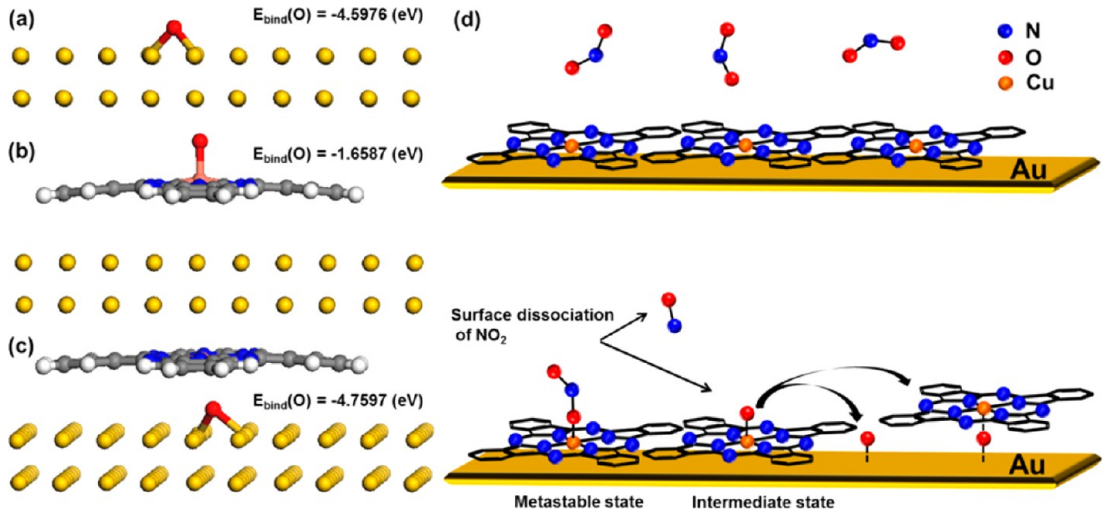

Figure 8. DFT models of CuPc/Au(111) with atomic O adsorbed on Au and CuPc layers. (a) Atomic O adsorbed on Au(111). (b) O−CuPc/Au(111) with O on top of the CuPc. (c) CuPc/O−Au(111) with O between CuPc and Au(111), i.e. subsurface adsorbate. (d) Suggested schematic diagram for domain fracture induced by NO_2 dosing.

atoms would be expected to migrate readily to sub-CuPc layer sites bound to Au or just to the Au(111) surface sites.

An analysis of the Bader charges in the DFT calculations is consistent with the higher binding energy of the O electrons in dissociation products observed in XPS. The O/CuPc/Au(111) Bader charge is 6.53 lel, and on transfer to the gold surface the O atoms gains about a quarter of an electron; the O/Au(111) Bader charge is 6.69 lel, and the CuPc/O/Au charge is 6.78 lel. This gain in electrons would induce a lower electron binding energy. The DFT calculations are consistent with a large thermodynamic driving force for O atoms dissociating from NO_2 on CuPc/Au(111) to diffuse to the Au(111) surface. These subsurface O binding sites should have very high thermal stability after their formation.

The high binding energy of O/Au(111) is consistent with the high thermal stability of the fractured islands and O only recombinatively desorbing from Au(111) above 200 °C.[61] This desorption temperature is similar to the annealing temperature where recovery of domain fracture occurs in Figure 3f (T_{rec} = 150 °C). The CuPc/O/Au sites are not directly observed by STM, because it is likely that subsurface O atoms do not significantly change the CuPc topography. This hypothesis is supported by DFT models of CuPc/O/Au which show that the heights of both the metal center and the rings change by less than 0.2 Å when the O atom is bound subsurface. However, even if O were chemisorbed between the CuPc molecules, this would be nearly impossible to detect since adsorbates on Au(111) cause only small corrugation in STM images, while the CuPc has a height of 1.7 Å on Au(111).[8]

4. DISCUSSION

A simplified model is proposed (Figure 8d) which is consistent with the sensing data, the STM data, and the DFT calculations. First, NO_2 molecules reversibly and molecularly chemisorb to the CuPc metal center and dissociate by an activated process into O and NO. It is noted that a surface bimolecular reaction is also possible ($2\ NO_2 \rightarrow NO + NO_3 \rightarrow NO + NO_2 + O$) since the experiments were performed at high concentration and not just high dose;[65] however, the net result of both the unimolecular and bimolecular reactions is chemisorption of O atoms. Subsequently, the atomic O diffuses to the Au(111) surface, which allows binding of more NO_2. The substrate-bound O atoms act as coadsorbates and induce a change in the CuPc domain structure, such as domain fracture and rearrangement of molecules. The molecular rearrangement and domain fracture likely occur because of the increased distance between adjacent CuPc molecules after O coadsorption. The eventual high density of O atoms per CuPc molecule could lower the barrier for lifting the CuPc from the Au surface and induce domain fracture or rearrangement. However, it also possible NO_2 molecules diffuse into the CuPc layer and are dissociated on the Au(111) surface with water in air, as shown in Figure S3 in the SI.[66,67] As shown in Figure 2a, there are gaps between CuPc molecules; therefore, the CuPc monolayer may not be able to block diffusion of the small NO_2 molecules. However, even though there is another channel generating atomic oxygen, this reinforces that atomic oxygen can be generated in CuPc/Au(111) and induce domain fracture.

The DFT calculations and XPS data are consistent with dissociating NO_2 to generate O atoms which adsorb on bare Au or insert into subsurface sites between CuPc molecules and Au(111). Also, the adsorption of atomic O between CuPc and the surface would probably induce a change in the CuPc spacing, which is typical of coadsorbates.[68,69] Due to this adsorption, the spacing between CuPc molecules increases or the MPc molecules rotate. These spacing changes between molecules induced by subsurface O adsorbates generate reorganization of CuPc molecules and the lattice mismatch shown in Figure 9. In Figure 9, lines are drawn along the rows of CuPc (green arrow). On clean surfaces, the molecules form perfect linear arrays (Figure 9a). However, on the NO_2-dosed CuPc monolayer, the molecules are aligned along only one direction (green arrow), while the CuPc molecules shift 1/2 unit cell almost every two molecules along the perpendicular direction (red line) in Figure 9b.

The NO_2-induced domain fracturing of CuPc layers (mono-, bi-, and multilayer) is consistent with the irreversible sensing response with CuPc chemFETs.[31,32] Charge carriers have their highest mobility inside the domains since they are nearly perfect single crystals, while the domain boundaries act as barriers to charge transport.[70−77] The NO_2 dosing increases the density of domain boundaries by domain fracture to further

dx.doi.org/10.1021/ja403752r | J. Am. Chem. Soc. XXXX, XXX, XXX−XXX

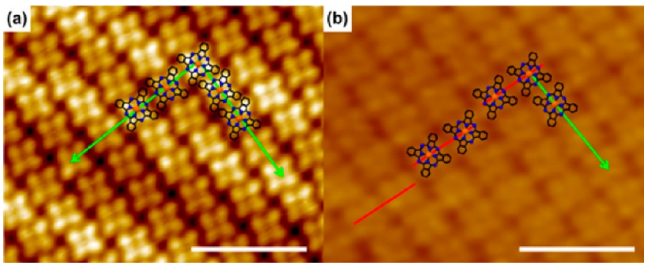

Figure 9. Empty-state STM images of a CuPc monolayer surface. Scale bars are 5 nm. (a) Clean CuPc monolayer (V_s = 2.0 V, I_t = 80 pA). (b) CuPc monolayer dosed with 10 ppm of NO_2 for 5 min at 25 °C and annealed at 50 °C for 20 min (V_s = 2.0 V, I_t = 40 pA). Lines are drawn along the rows of CuPc (green arrow). On clean surfaces, the molecules form perfect linear arrays. However, on the NO_2-dosed CuPc monolayer, the molecules are aligned along only one direction (green arrow), while the CuPc molecules shift 1/2 unit cell almost every two molecules along the perpendicular direction (red line).

isolate domains. Charge carriers require high energy to cross domain boundaries.[71,73] Since NO_2-induced domain fracture originates at the CuPc/Au interface, it is proposed the NO_2-induced domain fraction also degrades the CuPc/Au electrical contacts. It is well-known that the performance of OTFTs depends strongly on the interface between the organic layer and metal contacts.[78−81] In CuPc OTFTs exposed to high NO_2 doses, the increased density of domain boundaries would act to trap carriers near the contacts and induce positive uncompensated charge, which is consistent with the increased threshold voltage observed on NO_2 dosing.

5. CONCLUSION

Scanning tunneling microscopy (STM) was used to study ambient adsorption of NO_2 on CuPc monolayers and elucidate a molecular scale mechanism of NO_2 sensing for CuPc OTFT sensors. For low NO_2 exposures, isolated chemisorbates are observed on the CuPc metal centers. These chemisorbates are removed by annealing at 100 °C. However, for high NO_2 exposures, domain fractures appear in the CuPc film due to NO_2-induced reorganization. The NO_2-induced reorganization and domain fractures in CuPc are stable at 25 °C and can only be reversed by annealing above 150 °C. Such high stability indicates that the driving force for domain fracture originates from strongly bound adsorbates. The existence of atomic O on Au(111) after exposure to NO_2 is confirmed by XPS analysis. Therefore, the STM and XPS data are consistent with a dissociation of NO_2 and generation of an O−CuPc complex. As shown by DFT calculations, O binds stronger with subsurface sites on the Au(111) surface than with top of CuPc molecules. It is proposed that the migrated O atoms bound in between CuPc and Au induce domain fracture. The dissociation of NO_2 generates atomic O which adsorbs at the CuPc/Au interface. This mechanism is supported by studies of O_3 dissociative chemisorption on CuPc monolayers, as well as NO_2 dosing of bilayer and multilayer CuPc/Au(111), both of which show similar NO_2-induced domain fracture. These NO_2-induced reconstructions of domains on bilayers and multilayers are consistent with domain fracture being one important source for the irreversible V_{th} shifts observed in CuPc OTFTs. The types of mechanisms that lead to dosimetric sensing in the present instance (i.e., secondary surface reactions of analytes and sensor surface reconstruction) may serve as a model for the dosimetric sensing behavior in other OTFT chemical sensors, especially those which use metal phthalocyanines.

■ ASSOCIATED CONTENT

Supporting Information

Figures S1−S3. This material is available free of charge via the Internet at http://pubs.acs.org.

■ AUTHOR INFORMATION

Corresponding Author

akummel@ucsd.edu

Notes

The authors declare no competing financial interest.

■ ACKNOWLEDGMENTS

This work was supported by NSF Grant CHE-0848502 and STARnet, a Semiconductor Research Corporation program, sponsored by MARCO and DARPA.

■ REFERENCES

(1) Wright, J. D. *Prog. Surf. Sci.* **1989**, *31*, 1.
(2) Archer, P. B. M.; Chadwick, A. V.; Miasik, J. J.; Tamizi, M.; Wright, J. D. *Sens. Actuators* **1989**, *16*, 379.
(3) Ho, K. C.; Tsou, Y. H. *Sens. Actuators, B* **2001**, *77*, 253.
(4) van Faassen, E.; Kerp, H. *Sens. Actuators, B* **2003**, *88*, 329.
(5) Bohrer, F. I.; Colesniuc, C. N.; Park, J.; Ruidiaz, M. E.; Schuller, I. K.; Kummel, A. C.; Trogler, W. C. *J. Am. Chem. Soc.* **2009**, *131*, 478.
(6) Grate, J. W.; Klusty, M.; Barger, W. R.; Snow, A. W. *Anal. Chem.* **1990**, *62*, 1927.
(7) Kanai, M.; Kawai, T.; Motai, K.; Wang, X. D.; Hashizume, T.; Sakura, T. *Surf. Sci.* **1995**, *329*, L619.
(8) Lu, X.; Hipps, K. W.; Wang, X. D.; Mazur, U. *J. Am. Chem. Soc.* **1996**, *118*, 7197.
(9) Lu, X.; Hipps, K. W. *J. Phys. Chem. B* **1997**, *101*, 5391.
(10) Wang, Y. F.; Kroger, J.; Berndt, R.; Hofer, W. *Angew. Chem., Int. Ed.* **2009**, *48*, 1261.
(11) Zhang, L. Z.; Cheng, Z. H.; Huan, Q.; He, X. B.; Lin, X.; Gao, L.; Deng, Z. T.; Jiang, N.; Liu, Q.; Du, S. X.; Guo, H. M.; Gao, H. J. *J. Phys. Chem. C* **2011**, *115*, 10791.
(12) Li, Z. Y.; Li, B.; Yang, J. L.; Hou, J. G. *Acc. Chem. Res.* **2010**, *43*, 954.
(13) Schmidt, A.; Chau, L. K.; Back, A.; Armstrong, N. R. *Phthalocyanines* **1996**, *4*, 307.
(14) Eley, D. D.; Hazeldine, D. J.; Palmer, T. F. *J. Chem. Soc., Faraday Trans. 2* **1973**, *69*, 1808.
(15) Tegeler, E.; Iwan, M.; Koch, E. E. *J. Electron Spectrosc.* **1981**, *22*, 297.
(16) Schaffer, A. M.; Gouterman, M.; Davidson, E. R. *Theor. Chim. Acta* **1973**, *30*, 9.
(17) Figgis, B. N.; Kucharski, E. S.; Reynolds, P. A. *J. Am. Chem. Soc.* **1989**, *111*, 1683.
(18) Martin, M.; Andre, J. J.; Simon, J. *J. Appl. Phys.* **1983**, *54*, 2792.
(19) Kerp, H. R.; Westerduin, K. T.; van Veen, A. T.; van Faassen, E. E. *J. Mater. Res.* **2001**, *16*, 503.
(20) Simon, J.; André, J. J.; Lehn, J. M.; Rees, C. W. *Molecular Semiconductors: Photoelectrical Properties and Solar Cells*; Springer-Verlag: Berlin, New York, 1985.
(21) Zwart, J.; Van Wolput, J. H. M. C. *J. Mol. Catal.* **1979**, *5*, 51.
(22) Lever, A. B. P.; Wilshire, J. P.; Quan, S. K. *J. Am. Chem. Soc.* **1979**, *101*, 3668.
(23) Yahiro, H.; Naka, T.; Kuramoto, T.; Kurohagi, K.; Okada, G.; Shiotani, M. *Microporous Mesoporous Mater.* **2005**, *79*, 291.
(24) Honeybourne, C. L.; Ewen, R. J.; Hill, C. A. S. *J. Chem. Soc., Faraday Trans. 1* **1984**, *80*, 851.
(25) Bouvet, M.; Guillaud, G.; Leroy, A.; Maillard, A.; Spirkovitch, S.; Tournilhac, F. G. *Sens. Actuators, B* **2001**, *73*, 63.

(26) Bohrer, F. I.; Sharoni, A.; Colesniuc, C.; Park, J.; Schuller, I. K.; Kummel, A. C.; Trogler, W. C. *J. Am. Chem. Soc.* **2007**, *129*, 5640.
(27) Tran, N. L.; Bohrer, F. I.; Trogler, W. C.; Kummel, A. C. *J. Chem. Phys.* **2009**, *130*, 174305.
(28) Royer, J. E.; Kappe, E. D.; Zhang, C. Y.; Martin, D. T.; Trogler, W. C.; Kummel, A. C. *J. Phys. Chem. C* **2012**, *116*, 24566.
(29) Choi, C. G.; Lee, S.; Lee, W. J. *Sens. Actuators, B* **1996**, *32*, 77.
(30) Bishop, S. R.; Tran, N. L.; Poon, G. C.; Kummel, A. C. *J. Chem. Phys.* **2007**, *127*, 214702.
(31) Newton, M. I.; Starke, T. K. H.; Willis, M. R.; McHale, G. *Sens. Actuators, B* **2000**, *67*, 307.
(32) Newton, M. I.; Starke, T. K. H.; McHale, G.; Willis, M. R. *Thin Solid Films* **2000**, *360*, 10.
(33) Padma, N.; Joshi, A.; Singh, A.; Deshpande, S. K.; Aswal, D. K.; Gupta, S. K.; Yakhmi, J. V. *Sens. Actuators, B* **2009**, *143*, 246.
(34) Alagna, L.; Capobianchi, A.; Paoletti, A. M.; Pennesi, G.; Rossi, G.; Casaletto, M. P.; Generosi, A.; Paci, B.; Albertini, V. R. *Thin Solid Films* **2006**, *515*, 2748.
(35) Park, J.; Royer, J. E.; Colesniuc, C. N.; Bohrer, F. I.; Sharoni, A.; Jin, S. H.; Schuller, I. K.; Trogler, W. C.; Kummel, A. C. *J. Appl. Phys.* **2009**, *106*, 034505.
(36) Buchholz, J. C.; Somorjai, G. A. *J. Chem. Phys.* **1977**, *66*, 573.
(37) Kresse, G.; Furthmuller, J. *Comput. Mater. Sci.* **1996**, *6*, 15.
(38) Kresse, G.; Furthmuller, J. *Phys. Rev. B* **1996**, *54*, 11169.
(39) Blochl, P. E. *Phys. Rev. B* **1994**, *50*, 17953.
(40) Kresse, G.; Joubert, D. *Phys. Rev. B* **1999**, *59*, 1758.
(41) Perdew, J. P.; Burke, K.; Ernzerhof, M. *Phys. Rev. Lett.* **1996**, *77*, 3865.
(42) Perdew, J. P.; Burke, K.; Ernzerhof, M. *Phys. Rev. Lett.* **1997**, *78*, 1396.
(43) Henkelman, G.; Arnaldsson, A.; Jonsson, H. *Comput. Mater. Sci.* **2006**, *36*, 354.
(44) Sanville, E.; Kenny, S. D.; Smith, R.; Henkelman, G. *J. Comput. Chem.* **2007**, *28*, 899.
(45) Tang, W.; Sanville, E.; Henkelman, G. *J. Phys. Condens. Matter* **2009**, *21*, 084204.
(46) Marinelli, F.; Dell'Aquila, A.; Torsi, L.; Tey, J.; Suranna, G. P.; Mastrorilli, P.; Romanazzi, G.; Nobile, C. F.; Mhaisalkar, S. G.; Cioffi, N.; Palmisano, F. *Sens. Actuators, B* **2009**, *140*, 445.
(47) Nguyen, T. Q.; Escano, M. C. S.; Kasai, H. *J. Phys. Chem. B* **2010**, *114*, 10017.
(48) Lozzi, L.; Picozzi, S.; Santucci, S.; Cantalini, C.; Delley, B. *J. Electron Spectrosc.* **2004**, *137*, 101.
(49) Tran, N. L.; Kummel, A. C. *J. Chem. Phys.* **2007**, *127*, 214701.
(50) Wang, G. F.; Ramesh, N.; Hsu, A.; Chu, D.; Chen, R. R. *Mol. Simul.* **2008**, *34*, 1051.
(51) Buchner, F.; Seufert, K.; Auwarter, W.; Heim, D.; Barth, J. V.; Flechtner, K.; Gottfried, J. M.; Steinruck, H. P.; Marbach, H. *ACS Nano* **2009**, *3*, 1789.
(52) Bartram, M. E.; Koel, B. E. *Surf. Sci.* **1989**, *213*, 137.
(53) Wickham, D. T.; Banse, B. A.; Koel, B. E. *Catal. Lett.* **1990**, *6*, 163.
(54) Honeybourne, C. L.; Ewen, R. J. *J. Phys. Chem. Solids* **1983**, *44*, 215.
(55) Zheng, G.; Altman, E. I. *Surf. Sci.* **2000**, *462*, 151.
(56) Chen, H. L.; Wu, S. Y.; Chen, H. T.; Chang, J. G.; Ju, S. P.; Tsai, C.; Hsu, L. C. *Langmuir* **2010**, *26*, 7157.
(57) Yen, M. Y.; Ho, J. J. *Chem. Phys.* **2010**, *373*, 300.
(58) Mrwa, A.; Friedrich, M.; Hofmann, A.; Zahn, D. R. T. *Sens. Actuators, B* **1995**, *25*, 596.
(59) Sadaoka, Y.; Jones, T. A.; Revell, G. S.; Gopel, W. *J. Mater. Sci.* **1990**, *25*, 5257.
(60) Saliba, N.; Parker, D. H.; Koel, B. E. *Surf. Sci.* **1998**, *410*, 270.
(61) Parker, D. H.; Koel, B. E. *J. Vac. Sci. Technol., A* **1990**, *8*, 2585.
(62) vanDaelen, M. A.; Li, Y. S.; Newsam, J. M.; vanSanten, R. A. *J. Phys. Chem.* **1996**, *100*, 2279.
(63) Bogicevic, A.; Hass, K. C. *Surf. Sci.* **2002**, *506*, L237.
(64) Gurevich, A. B.; Bent, B. E.; Teplyakov, A. V.; Chen, J. G. *Surf. Sci.* **1999**, *442*, L971.
(65) Rodriguez, J. A.; Jirsak, T.; Liu, G.; Hrbek, J.; Dvorak, J.; Maiti, A. *J. Am. Chem. Soc.* **2001**, *123*, 9597.
(66) Wang, J.; Koel, B. E. *J. Phys. Chem. A* **1998**, *102*, 8573.
(67) Wang, J.; Voss, M. R.; Busse, H.; Koel, B. E. *J. Phys. Chem. B* **1998**, *102*, 4693.
(68) Kong, X. H.; Yang, Y. L.; Lei, S. B.; Wang, C. *Surf. Sci.* **2008**, *602*, 684.
(69) Batteas, J. D.; Dunphy, J. C.; Somorjai, G. A.; Salmeron, M. *Phys. Rev. Lett.* **1996**, *77*, 534.
(70) Anderson, P. W. *Phys. Rev.* **1958**, *109*, 1492.
(71) Horowitz, G.; Hajlaoui, M. E. *Adv. Mater.* **2000**, *12*, 1046.
(72) Chwang, A. B.; Frisbie, C. D. *J. Appl. Phys.* **2001**, *90*, 1342.
(73) Verlaak, S.; Arkhipov, V.; Heremans, P. *Appl. Phys. Lett.* **2003**, *82*, 745.
(74) Puntambekar, K.; Dong, J. P.; Haugstad, G.; Frisbie, C. D. *Adv. Funct. Mater.* **2006**, *16*, 879.
(75) Huang, H. C.; Wang, H. B.; Zhang, J. D.; Yan, D. H. *Appl. Phys. A* **2009**, *95*, 125.
(76) Kaake, L. G.; Barbara, P. F.; Zhu, X. Y. *J. Phys. Chem. Lett.* **2010**, *1*, 628.
(77) Wang, X. J.; Ji, S. L.; Wang, H. B.; Yan, D. H. *Org. Electron.* **2011**, *12*, 2230.
(78) Di Carlo, A.; Piacenza, F.; Bolognesi, A.; Stadlober, B.; Maresch, H. *Appl. Phys. Lett.* **2005**, *86*, 263501.
(79) Jin, S. H.; Jung, K. D.; Shin, H.; Park, B. G.; Lee, J. D. *Synth. Met.* **2006**, *156*, 196.
(80) Wang, S. D.; Miyadera, T.; Minari, T.; Aoyagi, Y.; Tsukagoshi, K. *Appl. Phys. Lett.* **2008**, *93*, 043311.
(81) Vinciguerra, V.; La Rosa, M.; Nicolosi, D.; Sicurella, G.; Occhipinti, L. *Org. Electron.* **2009**, *10*, 1074.